All-optical integrated optic devices: A hybrid approach

A. Driessen
H.J.W.M. Hoekstra
F. Horst
G.J.M. Krijnen
B.J. Offrein
J.B.P. van Schoot
P.V. Lambeck
Th.J.A. Popma

Indexing terms: Integrated optics device, Nonlinear, All-optical

Abstract: All-optical data processing is highly desirable in optical data-communication networks because of the increasing need of bandwidth and optical transparency. The paper presents an evaluation of integrated optics device concepts, discusses materials requirements and gives experimental results of own work on devices based on silicon technology with hybrid integration of polymers as a nonlinear material.

1 Introduction

Prediction of the future penetration of optical networks in the information society is quite a precarious task. It is even more arduous if one wants to know an exact time-table of the developments that finally could lead to fibre to the home, or even fibre to the desktop. In order to reach this advanced stage of development — probably in the second decade of the next century — one will need integrated optic modules that route, switch, multiplex and process multi-Gbit/s data traffic [1]. These devices will find use everywhere in the communication network, including in small companies and private homes, and thus will enter the consumer market. Consequently, these modules should be available at a low price and in large quantities, without concessions in performance and reliability.

2 Theoretical considerations

All-optical devices [2–6] can be considered as the optical equivalent of transistor-based elementary devices in electronic circuitry, for example logic gates and amplifiers. The devices enable the control or switching of a light beam by another one. Unlike electrons, which obey Fermi-statistics and show strong interaction, photon obey Bose statistics and do not interact directly. Interaction of photons is only possible with the aid of a suitable nonlinear optical (NLO) material. The first light beam introduces a change Δn of the index of refraction n of the material. Thereafter, this change can be probed by the second beam.

For a quantitative analysis of all-optical interaction, one conveniently starts with an expansion of the polarization $\mathbf{P}(\mathbf{r}, t)$ as a function of the incoming fields $\mathbf{E}_i(\mathbf{r}, t)$. Assuming a local and instantaneous nonlinearity one gets [7]:

$$\mathbf{P}(\mathbf{r},t) = \varepsilon_0\{\chi^{(1)}\cdot\mathbf{E}_1(\mathbf{r},t) + \chi^{(2)}\cdot\mathbf{E}_1(\mathbf{r},t)\cdot\mathbf{E}_2(\mathbf{r},t) + \chi^{(3)}\cdot\mathbf{E}_1(\mathbf{r},t)\cdot\mathbf{E}_2(\mathbf{r},t)\cdot\mathbf{E}_3(\mathbf{r},t) + \ldots\} \quad (1)$$

The coefficient $\chi^{(n)}$ denotes the nth order susceptibility. In the applications of interest for this paper, terms of higher order than three are neglected or treated as saturation effects of $\chi^{(3)}$. If the incoming fields can be represented by plane waves one can write:

$$P_i(-\omega_1) = \chi^{(1)}_{i,j}(-\omega_1;\omega_1)E_j(\omega_1) + \chi^{(2)}_{i,j,k}(-\omega_1;\omega_2,\omega_3)E_j(\omega_2)E_k(\omega_3) + \chi^{(3)}_{i,j,k,l}(-\omega_1;\omega_2,\omega_3,\omega_4)E_j(\omega_2)E_k(\omega_3)E_l(\omega_l) + \ldots \quad (2)$$

where a sum over all frequencies ω has to be performed and the Einstein convention of summing over double indices is used. Positive and negative frequencies denote the frequencies of the generating (ω) and generated ($-\omega$) electrical or polarisation fields. For all terms, the frequencies involved sum up to zero.

For application in all-optical devices, we focus mainly on the coefficients related to the Intensity-Dependent Refractive Index (IDRI). We start with the expression for the linear case.

$$n^2 = 1 + \chi^{(1)}_{i,j}(-\omega;\omega) \quad (3)$$

Assuming an isotropic medium and two electric fields $E(\omega_a)$ and $E(\omega_b)$ polarised along the 1-axis, for the nonlinear case with only third order effects one obtains [8]:

$$n^2(\omega_a) = 1 + \chi^{(1)}_{i,j}(-\omega_a;\omega_a) + 3\chi^{(3)}_{1,1,1,1}(-\omega_a;\omega_a,-\omega_a,\omega_a)|E_1(\omega_a)|^2$$

IEE Proceedings online no. 19982144

Paper first received 27th may 1995 and in final revised form 5th August 1997

The authors are with the Lightwave Device Group, MESA Research Institute, University of Twente, P.O. Box 217, 7500 AE Enschede, The Netherlands

$$+ 6\chi^{(3)}_{1,1,1,1}(-\omega_a;\omega_a,-\omega_b,\omega_b)|E_1(\omega_b)|^2 \quad (4)$$

In certain application fields and depending on the physical origin of the IDRI sometimes other terms are used. When two light beams are involved, for example, one often speaks about 'cross phase modulation' or, when the imaginary part of the index of refraction is changed 'cross gain modulation'.

If only one beam at one frequency is involved one obtains for the IDRI:

$$n = n_0 + n_{2,E}|E|^2 = n_0 + n_{2,I}I \quad (5)$$

with I the intensity and

$$n_{2,E} = (n_0\varepsilon_0 c/2)\cdot n_{2,I} \cong 3\chi^{(3)}_{1,1,1,1}/(2n_0) \quad (6)$$

In order to get some feeling for the values of the NLO coefficients and the intensities needed for all-optical switching one can calculate the intensity induced phase shift:

$$\Delta\Phi^{NL} = \frac{2\pi}{\lambda_0}\cdot n_{2,I}IL_{eff} \quad (7)$$

where L_{eff} is the effective length (for example, the length of a nonlinear branch in a Mach-Zehnder interferometer, MZI) over which the phase shift accumulates. For a device with approximately L_{eff} = 1cm complete switching (π phase shift) can easily be obtained for $n_{2,I}I = 10^{-4}$.

If the light by passing through L_{eff} is substantially absorbed by either one or two photon absorption, the intensity I in eqn. 7 will be reduced. The phase shift in eqn. 7 is therefore an upper bound. Stegeman and coworkers [4] introduced two figures of merit (FOM) W and T which should satisfy the conditions $W > 2$ and $T < 1$ in order to allow for a π nonlinear phase shift. For W (1-photon absorption) and T (2-photon absorption) they propose:

$$W = \Delta n_{sat}/(\alpha_0\lambda_0) \qquad T = 2\lambda_0\alpha_2/n_{2,I} \quad (8)$$

where the total absorption is given by $\alpha = \alpha_0 + \alpha_2 I$, Δn_{sat} is the change in n at saturation. Absorption not only diminishes the all-optical performance of the device, but also limits the light intensity that can safely be guided. Because of the strong concentration of light in the waveguide, average power levels of 10^{-2} to 10^{-1}W can result in irreversible thermal damage of waveguides with losses above 10dB/cm.

Recently, it was realised that the desired all-optical phase shift cannot only be obtained by third order nonlinearity, but also by utilising a cascaded process based on wavevector-mismatched second-harmonic generation (SHG) [5, 9]. The effect can be explained by up-conversion from ω to 2ω and down-conversion from 2ω to ω with non-zero wavevector mismatch. The phase fronts at ω and 2ω travel at different velocities, and the relative phase accumulated by the phase fronts upon down-conversion causes a net nonlinear phase-shift in the fundamental wave. it is possible to calculate the maximum phase-shift by using an effective IDRI coefficient $n_{2,I,eff}$ [10]:

$$n_{2,I,eff} = sign(\Delta\beta)\frac{4}{c\varepsilon_0}\frac{\left[d^{(2)}_{eff}\right]^2}{n^3}\frac{L}{\lambda} \quad (9)$$

where $\Delta\beta$ is the phase mismatch and $d^{(2)}_{eff}$ is the effective second order susceptibility coefficient. For practical use it is important to note that, unlike third order processes, the cascaded second order NLO process puts severe demands on the technology as accurate phase matching is necessary.

The nonlinear phase shift in eqns. 7 and 9 is proportional to the intensity and the interaction length. In this respect waveguiding structures have the great advantage that light is focused down to a few μm^2 and can propagate with low losses over large distances, for planar devices typically several centimetres. Using light pulses with a peak power of the order of 1W, power densities of 10^{11}–10^{12}W/m^2 can be obtained.

3 Materials aspects

Silicon and its oxides have been used for all-optical switching. Bieber *et al.* [11] demonstrated all-optical switching in a metal-semiconductor-metal waveguide structure. They measured a response time of 1 – 5ns. Liu *et al.* [12] used the free-carrier plasma effect in an asymmetric silicon Fabry-Perot (FP) etalon and could detect all-optical modulation at frequencies up to 0.5GHz. Henary *et al.* [13] found substantial enhancement of the third order NLO coefficient of porous silicon in comparison to crystalline silicon. They could demonstrate all-optical switching with a response time of about 1μs. Silica, SiO_2, which is the basic material for the standard telecommunication fibre, exhibits nonlinear switching effects at light intensities of only a few mW. The reason for this is the low absorption that allows the accumulation of the NLO phase shift over many kilometres.

In planar technology and multi-gigabit/s data streams at wavelengths relevant for telecommunication (1.3 and 1.5μm), the NLO coefficients of Si-based materials seem to be insufficient to enable realistic all-optical devices. Instead other materials have to be added in a hybrid approach in order to obtain the desired NLO behaviour, see also [5]. Table 1 gives a list of interesting materials with their linear and nonlinear properties and their figures of merit. For practical applications the response time τ is also of primary importance, because only materials that allow multi-Gbit/s data processing ($\tau \leq 10^{-9}$s) will enable serious alternatives for electronic devices. All-optical devices, that already have been demonstrated in fibre or semiconductor technology [14], should even open the route to 0.1 – 1Tbit/s data processing. At these high frequencies, the use of electronic devices is increasingly difficult or even impossible.

Table 1 gives four classes of materials: semiconductors, glasses, organics and composites. Semiconductors applied in a Semiconductor Optical Amplifier (SOA) exhibit very promising all-optical switching behaviour [15] but cannot easily be integrated in multi-functional integrated optic devices. Glasses exhibit values for the NLO coefficient too low for the relatively short interaction distances on a planar optical device. Organic materials show promising properties. The NLO properties have a pure electronic origin and are in consequence very fast ($\tau < 10^{-12}$). In many cases the material can relatively easily be processed in thin layers and is compatible with silicon technology. Single-crystal polydiacetylene channel waveguides have been fabricated that exhibit a nonlinearity $n_{2,I} = 3 \times 10^{-15}$m^2/W. This is a sufficiently high value to allow all-optical switching at low power levels [16] (less than 1W with a device length of ~ 1cm). Measurements on near resonant polydiacetylene 9-BCMU thin films reveal a value

Table 1: Linear and nonlinear optical constants of materials for application in all-optical switching devices

	λ, μm	α_0, m^{-1}	β_2, mW^{-1}	$n_{2,I}$, m^2W^{-1}	Δn_{sat}	τ, s	W	T	ref.
Semiconductors									
GaAs	1.06	10^2	2.4×10^{-10}	$<-3 \times 10^{-17}$	-3×10^{-4}		<2.8	>17	a
AlGaAs	1.56	10^1	6×10^{-13}	10^{-17}	6×10^{-5}	$<10^{-12}$	4	0.2	a
AlGaAs	0.81	2×10^3	2×10^{-10}	4×10^{-16}	4×10^{-3}		2.5	0.9	a
idem	0.85	5×10^1	2×10^{-10}	-3×10^{-17}	3×10^{-4}		7.1	11	a
Glass									
SiO_2	>1.06	10^{-4}	$<<10^{-14}$	3×10^{-20}	10^{-7}	10^{-14}	<1000	<<1	a
Pb doped	>1.06	0.5	$<10^{-13}$	4×10^{-19}	$>4 \times 10^{-6}$		>7.5	<0.7	a
RN (Corning)	1.06	1	$<6 \times 10^{-14}$	1.3×10^{-18}	1.4×10^{-5}		13	<0.1	a
Organics									
Crystalline PTS	1.06	8×10^1	6×10^{-10}	-5×10^{-16}	5×10^{-3}	2×10^{-12}	60	2.4	a
Amorphous PTS	1.06	8×10^1	10^{-9}	-10^{-16}	10^{-3}		13	23	a
Poly-4BCMU	1.3	2×10^2	$<2 \times 10^{-12}$	5×10^{-18}	7×10^{-5}		0.3	<1.0	a
Poly-9BCMU	0.71	4×10^4	1.8×10^{-8}	3.2×10^{-15}	7×10^{-5}		0.003	5	b
idem	0.64	9×10^4	$<9 \times 10^{-10}$	1.9×10^{-14}	7×10^{-5}		0.002	<0.06	b
DANS	1.06	$<10^2$	10^{-11}	2×10^{-17}	1.5×10^{-4}		>1.4	1	a
Composites									
CdS_xSe_{1-x} doped glass				-10^{-15}	0.001	10^{-10}			c
Embedded nano-particles of noble metals	λ_p^*			4×10^{-4}					c

λ_p^* is the wavelength at plasmon resonance
Data are taken from a, Stegeman and Miller [4], b, Molyneux *et al.* [17] and c, Hoekstra *et al.* [7]

nearly an order of magnitude higher [17]. But still much materials engineering has to be done, as acceptable values for the NLO coefficients or the reaction time are often found in materials with large absorption or low values for Δn_{sat}.

A possible solution would be to tailor special composite materials, where quantum size effects and local field enhancement would allow substantially higher NLO coefficients. The effect of absorption and therefore the requirements of the FOMs could be substantially reduced by introducing optical gain in the nonlinear waveguiding structures. Erbium doped planar waveguides with a gain of typically 3–6dB/cm ($-\alpha_0 = 70 - 140 m^{-1}$) have been demonstrated [18, 19] and show the feasibility of such an approach. The Er-doped waveguide itself can be used for all-optical switching. In the case of an Er-doped fibre amplifier, Myslinski *et al.* [20] reported gain switching with a response time of 20ns. One could apply this concept also in planar devices.

4 Design of all-optical integrated optic devices

From the above considerations, it is obvious that all-optical devices should make maximum use of the nonlinear properties of the materials. A careful design of the devices can provide the desired functional behaviour by optimally exploiting the available materials and technology. Realistic and reliable computer simulations have to be performed which include all relevant linear and nonlinear materials parameters and the geometry of the waveguiding structure. In the case of z-invariance, possibly with small perturbations, a nonlinear coupled-mode analysis (CMA) can be applied. For structures with non-periodic variations in the propagation direction, nonlinear beam-propagation methods (BPM) are more generally applicable. Nonlinear CMA and the two-dimensional nonlinear Fourier Transform- and Finite Difference-BPM (FT-BPM and FD-BPM) [21, 22] were used extensively. Real world three-dimensional problems can be linked to the analysis methods by means of the Nonlinear Effective-Index Method [23]. For a detailed understanding of the dynamic behaviour of all-optical switching of short pulses, for example soliton pulses, it is necessary to follow the electromagnetic field in space and time. With this aim Horst *et al.* [24–26] developed a nonlinear Time Domain BPM (TD-BPM). This method allows simulation of the nonlinear propagation of short pulses with nanometre and femtosecond resolution including all reflections at the individual grooves of a corrugation grating.

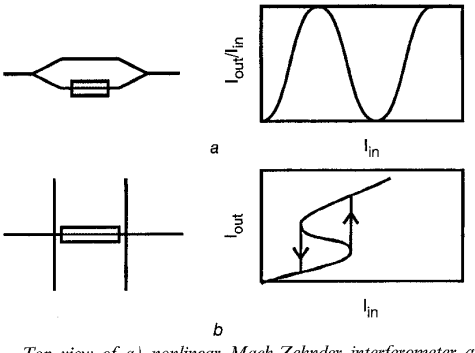

Fig. 1 *Top view of a) nonlinear Mach-Zehnder interferometer and b) nonlinear Fabry-Perot resonator and their input-output characteristics*
I_{in}; input intensity, I_{out}; output intensity grey areas; region of NLO waveguides

A large variety of all-optical integrated optic devices that make use of the IDRI have been proposed and demonstrated, see Figs. 1–3. In all-optical devices, the IDRI can introduce phase shifts ($\Delta\Phi$), changes in the

modal propagation constant $\Delta\beta$ and changes in the modal field profiles. Phase changes can be made effective by interference in a MZI, a FP etalon, or distributed couplers using gratings as well as prisms. Other devices like a grating mode converter or a Y- or X-junction depend critically on the modal propagation constant. Power dependent field changes are in general too small to be used in planar waveguide switches. The only exceptions seem to be devices using spatial solitons. With a suitable geometry most devices can be designed to perform various functions; they may act as all-optical switches, memories, logic switches, limiters, isolators or amplifiers.

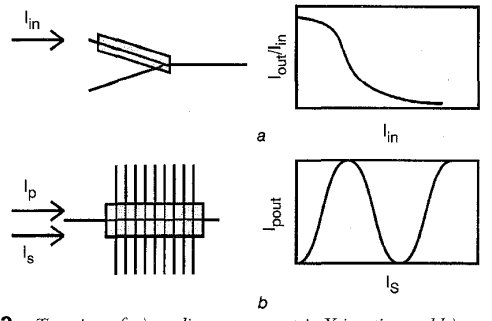

Fig. 2 *Top view of a) nonlinear asymmetric Y-junction and b) nonlinear grating mode converter and their input-output characteristics*
I_{in}; input intensity, I_{out}; output intensity, I_p; intensity pump beam, I_s; intensity signal beam, grey areas; region of NLO waveguides

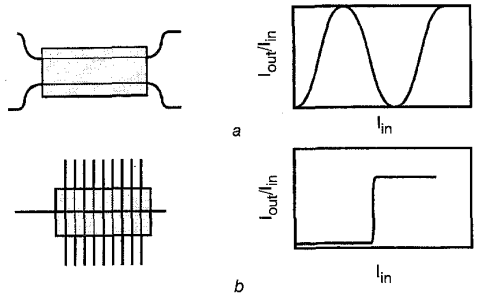

Fig. 3 *Top view of a) nonlinear directional coupler and b) soliton switch based on a nonlinear Bragg reflector and their input-out characteristics*
I_{in}; input intensity, I_{out}; output intensity, grey areas; region of NLO waveguides

All-optical devices, which in principle can be realised in (hybrid) integrated optic structures, are discussed in more detail. Krijnen [27] has done extensive computer simulations (nonlinear CMA and BPM) on three different nonlinear integrated optic devices: the nonlinear MZI [28] in Figs. 1*a* and 4, the nonlinear asymmetrical Y-junction (NAY) in Fig. 2*a* and the nonlinear grating mode converter (NGMC) in Fig. 2*b*.

The NMZI is based on the general principle of a MZI. A given input is divided into two equal beams which, by a certain interaction, incur a phase difference. By combination of the two beams, interference effects translate the phase difference to an output power variation. In the NMZI discussed here, additional inputs and outputs are added to the regular MZI, (Fig. 4). They are connected to the interferometer section by means of asymmetric Y-junctions. Moreover, the branches of the NMZI are bi-modal instead of mono-modal and are assumed to be nonlinear (in fact, the complete structure could be made of nonlinear waveguides). In the given set-up a probe beam (P_P) is launched in the central input waveguide and equally divided over the two branches. The asymmetric input Y-junctions convert the P_P input into fundamental modes of the MZI-branches. At the end of the branches these fundamental modes selectively propagate to the centre output symmetrical Y-junction. There they are recombined into fundamental and first order modes. The latter radiates out of the structure since the central output is mono-modal. Additional input signals (P_s^a and P_s^b) are fed into the MZI-branches as first order modes by means of the asymmetrical input Y-junctions. Using different modes there will be no phase-dependence of the switch even when probe and input signals are at the same wavelength and have the same polarisation direction. Inside the branches, crossphase modulation of the signal and probe beams induces mutual nonlinear phase changes. At the output side the signals are separated from the probe beams again by means of the mode-selective asymmetric Y-junctions. This way they do not pollute the output and, moreover, they can be used in cascaded devices. By virtue of the polarisation and wavelength independence of cross-phase modulation, NMZIs can perform several functions. They can find application as polarisation- and wavelength-converters, as (differential) amplifiers, logic gates and even pulse-reshapers.

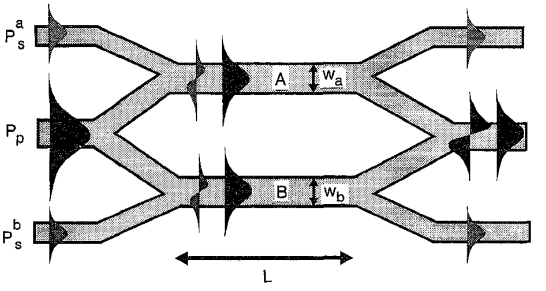

Fig. 4 *Top view of nonlinear Mach-Zehnder interferometer, NMZI*

The nonlinear asymmetric Y-junction is based on power dependent propagation constants. Assuming a positive (negative) IDRI, the input power is launched into the smallest (widest) branch of the junction in this device. Due to the IDRI, the propagation constant of the launched mode will increase (decrease) with power. Therefore, the initial difference in propagation constants of the modes of both branches will decrease, change sign and increase again. Since in asymmetric Y-junctions the mode with highest (lowest) propagation constant at the input will be converted to the fundamental (first order) mode of the output, the modal power distribution at the output will be power dependent. This modal power distribution can be converted into a measurable and useful output power variation employing a second asymmetric Y-junction (in opposite orientation) for mode splitting. One of the advantages of NAYs is that they do not have an oscillatory response. This makes them well suited for digital like operations (for example, logic gates). The device operation can be further extended by using an additional input signal in the second branch. In this case, the modal power distribution at the output will depend on the difference of both input powers.

The nonlinear grating mode converter is also based on power-dependent propagation constant changes.

This device makes use of a symmetric grating to couple a fundamental mode to a second order mode. The symmetry of the structure assures that neither the fundamental nor the second order mode couples with the first order mode. The grating period and length can be chosen such that for a given input power (I_p) all power is coupled to the second order mode at the output. On launching additional signal power in the first order mode the coupling between the fundamental and second order mode is detuned and the fundamental mode output power increases.

Fig. 5 gives a comparison (based on FD-BPM simulations) of the switching efficiency. All three devices exhibit switching at nearly the same normalised input level (within a factor of two) and the MZI appears to be the most efficient one.

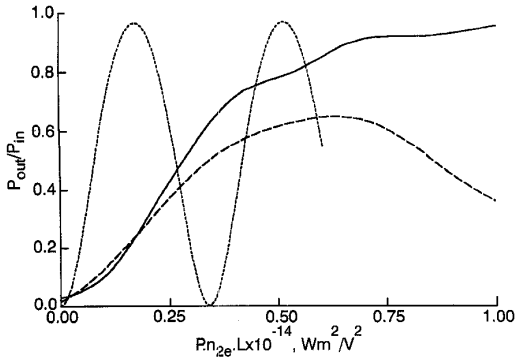

Fig. 5 *Comparison of nonlinear three all-optical switching devices*
Output power/input power is plotted against normalised input power
—— NAY
..... NMZI
---- NGMC

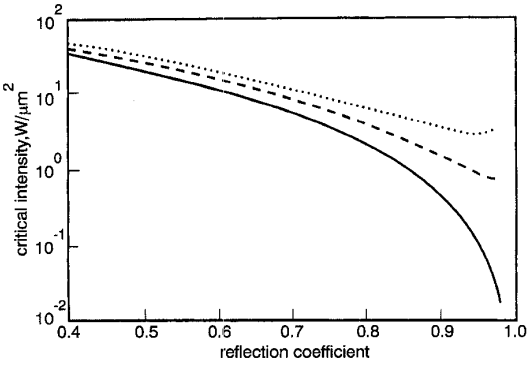

Fig. 6 *Critical incident intensity versus Fabry-Perot reflection coefficient for a length of L_i = 500 μm and for various values of absorption and nonlinearity $n_{2,I} = 10^{-17} m^2/W$*

The integrated optic NLO Fabry-Perot resonator has been studied extensively by Offrein [29]. He considers a resonator with a NLO material inside the resonator. Fig. 6 gives his results for the critical incident intensity P_{in} needed for observing bi-stability as a function of resonator losses. Assuming a standard channel waveguide, a loss of 2dB/cm and a resonator of length 1 mm one gets: $\alpha \cdot L = 0.05$. Therefore, similar to the case of the MZI, light power of about 10W should be sufficient to obtain switching for $n_{2,I} = 10^{-17} m^2/W$.

For applications, it is of importance that (all-optical) devices switch pulses as a whole. The devices considered up to now work properly only with pulses having a strictly rectangular shape. If one considers realistic pulses, it is easy to see that the devices will perform differently on the flanks of the pulse with low intensity and on the central part with high intensity. Severe pulse shape deformation (PSD) can therefore occur which inhibits further cascading of all-optical devices without pulse regeneration. In the following section, experiments are described which use PSD for measuring the nonlinear behaviour of experimental devices. PSD is absent if one works either with truly binary pulses having only two intensity levels (these are increasingly difficult to obtain as the pulse length decreases) or with solitons.

Temporal solitons, extremely stable pulses, can be obtained if light pulses with a sufficient intensity pass through a medium having a Kerr non-linearity $n_{2,I}$ and dispersion $k'' = \partial^2 k/\partial^2 \omega$, where k is the wavevector and ω the frequency of the light. Solitons have a characteristic length, the soliton length z_0, which is approximately the propagation length needed for a soliton to recover from a perturbation.

$$z_0 \propto t_s^2/k'' \tag{10}$$

where t_s is the soliton pulse duration. Complete switching without PSD can be obtained if the length of the switch is larger than z_0. In fibre devices the soliton length is on the order of kilometres. In a planar soliton device, z_0 should be reduced to a few centimetres. As one can see from eqn. 10, this can be obtained by working with very short pulses, in the range of ps or shorter, and with high dispersion. High dispersion in a device can be the result of the choice of a material. The high dispersion, however, needed for switching of picosecond pulses in a planar device can only be obtained by dispersive elements like gratings or coupled waveguides. The intensity needed to generate a soliton is inverse proportional to $n_{2,I}$.

Horst *et al.* [25, 26] have designed a soliton switch on the basis of Bragg solitons. A pulse entering the Bragg region will be reflected at low intensity. At high intensity a soliton is generated, which can pass through the Bragg region. Simulations with the TD-BPM, (Figs. 7 and 8) show that with $n_{2,I} = 10^{-17} m^2/W$ a threshold pulse peak power of less than 50W is sufficient to generate a soliton with $t_s \cong 1$ ps.

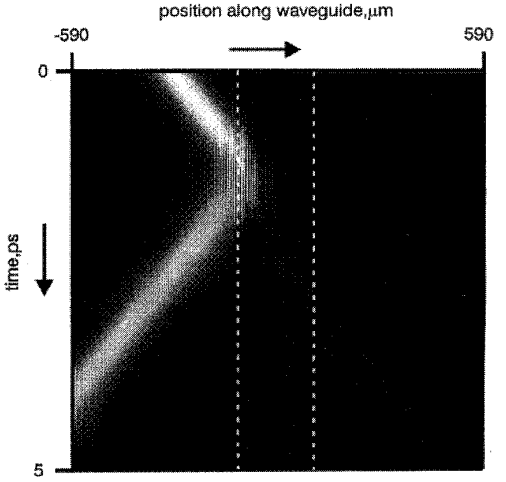

Fig. 7 *Time domain BPM simulation of a soliton switch based on a nonlinear Bragg reflector*
Input pulse intensity 15% below threshold, only reflection can be observed

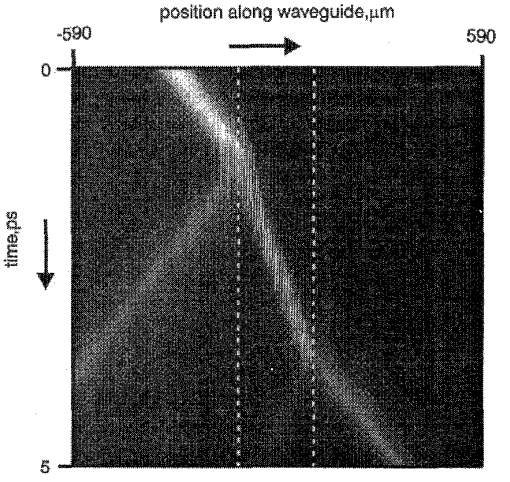

Fig. 8 *Time domain BPM simulation of a soliton switch based on a nonlinear Bragg reflector*
Input pulse intensity 15% above threshold, a compressed lightpulse (soliton) can propagate through the grating region

5 Experimental work on all-optical hybrid integrated optic devices

Several promising devices have been discussed, which should allow the demonstration of all-optical switching. For realisation, however, one will expect severe restrictions due to the lack of optimal materials up to now. Most of the materials considered in Table 1 do not have the required values for the figures of merit W and T. The difficulties related to the linear absorption (FOM W) can in part be circumvented by working with high power laser pulses as long as no thermal damage of the waveguide is introduced. Therefore, for critical measurements laserpulses with a large peak to average power relation should be employed. These enable an efficient use of the nonlinearity without introducing thermal damage.

Organic nonlinear materials like polymers can easily be combined with inorganic waveguides to form waveguiding layer structures on silicon wafers, e.g. Thakur and Krol [30] and Bartuch *et al.* [31]. When the NLO material is used as a cladding layer, the device can be nearly completely processed in the standard technology for linear optical devices. By etching, the linear cladding can be locally removed and the organic NLO material can easily be applied, for example by spincoating. As an additional advantage the technological demands on thickness homogeneity and surface roughness of the NLO material are greatly reduced. For the design of the waveguiding layer structure it is convenient to define an efficiency parameter Q_2 that relates the change in effective index of the layer structure ΔN_{eff} to the intensity I.

$$Q_2 = \frac{\Delta N_{eff}}{I \cdot n_{2,I}} \tag{11}$$

Van Schoot *et al.* [32, 33] worked with hybrid waveguide structures based on SiO_xN_y, deposited by chemical vapour deposition (CVD). They optimised Q_2 for a SiO_xN_y mono-modal waveguide with a polymer cladding. For this they applied a high refractive index Si_3N_4 layer by low pressure CVD on top of the guiding layer which 'pulls' the field towards the cladding. This layer is also helpful for etching a window in the cladding layer because the low index SiO_xN_y layer (deposited by plasma enhanced CVD with n = 1.65, index matched to the nonlinear polymer) is etched 50 times faster than the high index Si_3N_4 layer. The resulting structure is depicted in Fig. 9. This waveguiding structure has been used to fabricate an NMZI [34] and straight nonlinear waveguides for the determination of the two photon absorption (TPA).

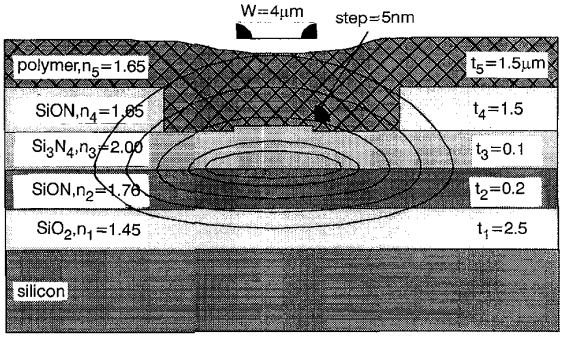

Fig. 9 *Cross section of channel structure used for the MZI and two photon absorption measuring device*
Intensity profiles give impression of modal field distribution

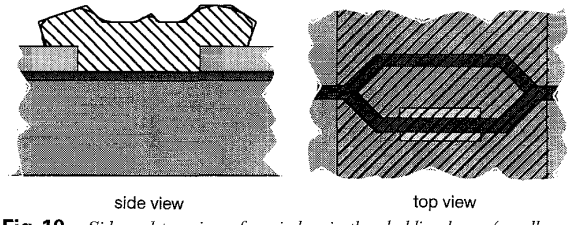

Fig. 10 *Side and top view of a window in the cladding layer (small rectangular region in top view) filled with nonlinear polymer (hatched area)*

For the NMZI, the cladding of one of the two branches (for the TPA device a part of the channel) has been removed, see Fig. 10. This window is filled with nonlinear polymer (Akzo-Nobel DANS side-chain polymer) using a spin-coating technique. The devices use mono-modal channel waveguides with a width of 2.5μm and an effective index contrast for the waveguide of 0.004.

For both devices, the MZI as well as the TPA measuring device, the nonlinear behaviour is observed by PSD. In most cases, this deformation is an unwanted effect. In our experiment, however, we used it to analyse the nonlinear behaviour of our devices. We start with bursts of 100ps full width at half maximum (FWHM) pulses from a mode-locked Q-switched Nd:YLF laser (λ = 1053nm) at a burst repetition rate of 134Hz. With the aid of a pulse picker the highest intensity pulse in the pulse train is selected. This results in high intensity pulses with a very low average power (75% of power in the high intensity pulses). A sampling oscilloscope (bandwidth 50GHz) is triggered on the high intensity pulses. The scope measures simultaneously the input and output pulses of the device under test. In this way the determination of the PSD is made nearly insensitive to fluctuations in the incoming laser pulses. Because of the relatively small PSD, the limits in bandwidth of the photodetector and oscilloscope, and the noise in the signal, the PSD is analysed in terms of only one parameter, the FWHM pulse width. The PSD can be defined by:

$$PSD = (FWHM_{out} - FWHM_{in})/FWHM_{in} \tag{12}$$

A nonlinear device with an increased throughput at high intensities will yield a sharpened output pulse and consequently a smaller FWHM. For a reduced throughput a flattened output pulse can be expected and thus a larger FWHM.

The PSD in the nonlinear MZI results in a positive or negative change in the FWHM pulse width depending on the linear phase difference between the fields in the two branches of the device. In Fig. 11 the expected PSD for an ideal MZI and a realistic one with a 10dB extinction ratio as a function of the phase difference Φ between the two branches for low intensities are given. For illustration, the linear transmittance of the MZI is given as a function of Φ. The PSD reaches its theoretical maximum for an infinite extinction ratio at $\Phi = \pi$. At this point the transmission is approaching zero. For a realistic MZI the extrema for the PSD are shifted away from the $\Phi = \pi$ point and are largely reduced.

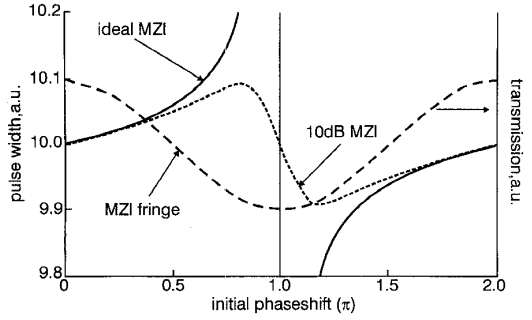

Fig. 11 *Simulation of transmission (dashed line) and nonlinear pulse shape deformation (change in FWHM pulse width) as a function of linear (low intensity) phase difference of the NMZI*

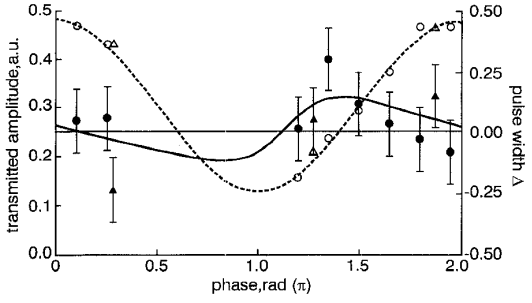

Fig. 12 *Nonlinear pulse shape deformation (relative change in FWHM pulse width) as a function of linear (low intensity) phase difference of the NMZI*

Solid circles and triangles represent experimental data. Solid line shows best fit to data points. Phase of Mach-Zehnder at experimental points was determined by linear transmission amplitude. Open triangles and circles represent experimental points. Dotted line shows theory

The experimental results of the NMZI are given in Fig. 12. The sample was cycled in temperature in order to change the initial phase Φ. The linear transmission was measured simultaneously with the PSD. This allowed to determine the phase Φ for each experimental point (open circles and triangles). The PSD was determined and plotted as solid circles and triangles. The next step is the determination of the intensity induced phaseshift of the NMZI. For this aim, simulations were performed as given in Fig. 11. The TPA is neglected here as it contributes only for a few percent to the observed PSD. The best fit of our simulation model to the experimental data, solid line in Fig. 12, is obtained for an intensity-induced phase shift of 0.5 rad for a peak power of 11.3W. This corresponds to a switching fraction of 23% for the pulse peak. This result allows a determination of the value for the NLO coefficient of the Akzo–Nobel DANS side-chain polymer $n_2 I = 12 \times 10^{-18} m^2/W$ in agreement with the value of $7 \times 10^{-18} m^2/W$ by Marqes *et al.* [35].

For the determination of the TPA-coefficients [33, 36] similar PSD measurements are performed on two channel waveguides with a length of 5cm. These waveguides (like the nonlinear MZI) were made in a first step from material with negligibly small nonlinear coefficients. In waveguide sections, with lengths of 1 and 4cm, the linear cladding (SiON) has been exchanged with NLO material (Akzo-Nobel DANS side-chain polymer). A relative pulse width of 99% could be measured at low pulse power indicating completely linear response. That means, no change could be detected within the experimental error. At high power, 106% and 112% are measured for the 1 and 4cm device respectively. By evaluation of the data a TPA coefficient $\beta_{m,DANS} = 4 \pm 2$pm/W could be obtained in reasonable agreement with the value of Stegeman and Miller [4] of 10pm/W.

Horst *et al.* [26, 36, 37] performed TPA measurements on a hybrid DANS side-chain polymer waveguiding structure. 1 ps pulses of a mode-locked dye-laser synchronously pumped by the Nd:YLF laser at 930nm were used. The PSD was studied by analysing autocorrelation traces. Fig. 13 gives the autocorrelation traces after transmission through a linear (Si-based materials) and a nonlinear waveguide (with DANS). From the observed pulse broadening a value of $\beta_{m,DANS} = 4.7 \pm 2$pm/W could be derived.

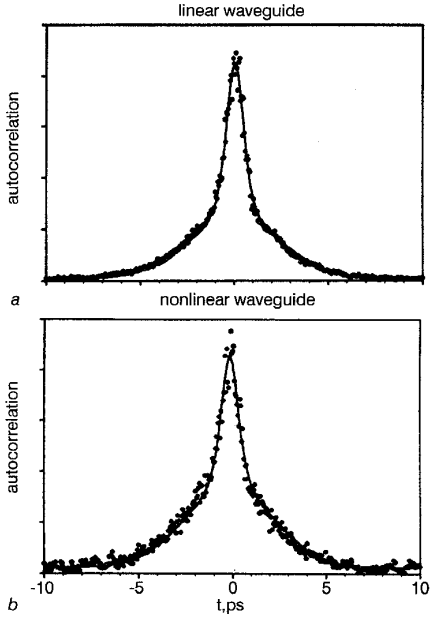

Fig. 13 *Autocorrelation traces of transmission of 1.5ps pulses through a linear and nonlinear waveguide*

Offrein [29] worked on the realisation of an integrated optic Fabry-Perot resonator as an all-optical switching device. The device was designed for all-optical switching of 80 ps pulses of a modelocked Nd:YLF laser at 1313 nm. The Fabry-Perot cavity is made from a channel waveguide in SiON technology on an Si-wafer, see Fig. 14. On top of the SiON waveguiding layers a NLO polymer (Akzo-Nobel DANS side-chain

polymer) is applied by spincoating. Optical feedback is obtained by two gratings made by holographic techniques on top of the waveguide. The dimensions and reflectivity are chosen in such a way that the delay time in the cavity is less than the pulse width of 80ps. With a finesse of about 30 the Fabry-Perot cavity length therefore should be in the order of 1mm.

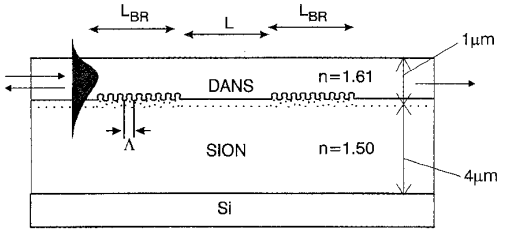

Fig. 14 *Cross section of integrated optic Fabry-Perot resonator*
L is the length of the Fabry-Perot cavity. L_{BR} is the length of the Bragg grating region

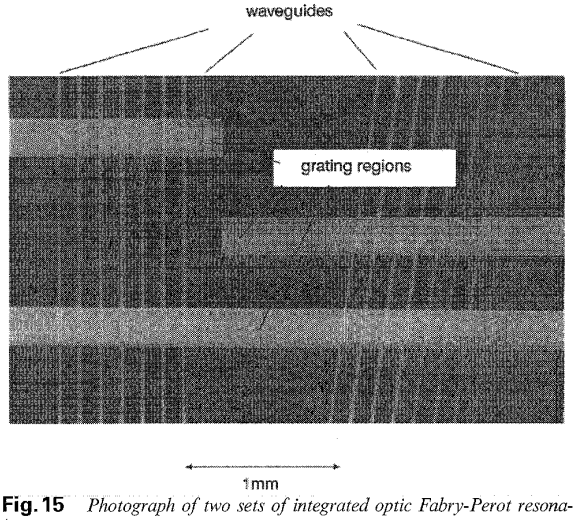

Fig. 15 *Photograph of two sets of integrated optic Fabry-Perot resonators*

The realisation of the Bragg-reflectors puts high demands on the technology, as the grating reflectors should operate in first order to prevent the excitation of radiant modes. For the grating period Λ_{BR} one therefore gets: $\Lambda_{BR} = \lambda/2n_{eff}$. This results in a desired grating period of approximately 400nm. The gratings are made by reactive ion etching of a resist layer, developed after holographic exposure by a UV argon-ion laser. Fig. 15 shows a series of devices. The channel waveguides with the two grating regions are clearly visible. The devices show the expected linear Fabry-Perot characteristics at low light intensities. Work with the high power Nd:YLF laser is in progress.

6 Final remarks

Having considered the different aspects of hybrid nonlinear integrated optic devices, one may draw the following conclusions:

(i) The feasibility of this class of devices has been shown by simulations and experiments. Several classes of all-optical devices have been designed and experimentally verified. Computer simulations allow the quantitative analysis of realistic devices. In cases where experimental work has been performed, good agreement is found between the experimental results and the computer analysis.

(ii) The nonlinear coefficients of silicon or Si-based inorganic compounds are probably too low for realistic planar high speed all-optical devices. Other materials, like organic polymers, show significantly better performance with respect to magnitude and response time of the nonlinear effects. A combination of these materials and silicon based waveguldes in a hybrid approach has already resulted in the demonstration of all-optical switching effects.

(iii) The nonlinear organic materials available up to now show promising properties. Their time response allows picosecond and even sub-ps all-optical switching corresponding to a bandwidth above 1 THz. The magnitude of the nonlinear coefficients, however, is such that unrealistically high pulse power is needed for complete switching. Many materials aspects have to be improved, but experimental results on PTS single crystal films and poly 9-BCMU give confidence that the ultimate limit in performance has not yet been reached.

(iv) For further optimisation of all-optical devices one could use more sophisticated approaches for the active materials. The nonlinear properties could be enhanced by using composites, nano-structures which exhibit quantum-size effects and the combination of gain and nonlinear behaviour. The latter concept has been shown to lead to very good performance in all-optical switching of bit-streams in the Gbit/s range in the case of semiconductor optical amplifiers.

7 Acknowledgments

The authors acknowledge helpful discussions with Dr. H. Albers, Dr. R.M. de Ridder and the technical support by Mr. A. Hollink and Mr. H. van Wolferen. The work has been partly supported by Akzo Nobel, IOP-special polymers of the Dutch Ministry of Economic Affairs, and the Netherlands Technology Foundation (STW).

8 References

1 GREEN, P.E., Jr.: 'Optical networking update', *IEEE J. Sel. Areas Commun.*, 1996, **14**, (5), pp. 764–779
2 ISLAM, M.N.: 'Ultrafast switching with nonlinear optics', *Phys. Today*, May 1994, pp. 34–40
3 STEGEMAN, G.I., and WRIGHT, E.M.: 'All-optical waveguide switching', *Opt. Quantum Electron.*, 1990, **22**, pp. 95–122
4 STEGEMAN, G.I., and MILLER, A.: 'Physics of all-optical switching devices' *in* MIDWINTER, J.E. (Ed): 'Photonics in switching' (Academic Press, 1993), vol. 1, chapter 5, pp. 81–145
5 STEGEMAN, G.I., and TORUELLAS, W.E.: 'Nonlinear materials for information processing and communications', *Phil. Trans. R. Soc. Lond. A*, 1996, **354**, pp. 745–756
6 SMITH, K., LUCEK, J.K., MANNING, R.J., and BLOW, K.J.: 'Advances in nonlinear optics for information processing and all-optical networking', *Phil. Trans. R. Soc. Lond. A*, 1996, **354**, pp. 707–717
7 HOEKSTRA, H.J.W.M., KRIJNEN, G.J.M., DRIESSEN, A., LAMBECK, P.V., and POPMA, TH.J.A.: 'Non-linear optics for transducers: principles and materials', *Sens. Actuators*, 1992, **34**, pp. 179–192
8 HOPF, F.A., and STEGEMAN, G.I.: 'Applied Classical Electrodynamics, Volume II: Nonlinear Optics' (John Wiley, New York 1986), pp. 100 ff
9 ASSANTO, G., STEGEMAN, G.I., SHEIK-BAHAE, M., and VANSTRYLAND, E.: 'Coherent interactions for all-optical signal processing via quadratic nonlinearities', *IEEE J. Quantum Electron.*, 1995, **31**, pp. 673–681

10 STEGEMAN, G.I., TORUELLAS, W., SUNDHEIMER, M., KIM, D., KRIJNEN, G.J.M., BAEK, Y., TREVINO-PALACIOS, C., VANSTRYLAND, E., SCHIEK, R., ASSANTO, G., TORNER, L., MENYUK, C., BIERLEIN, J.D., SOHLER, W., VIDAKOVIC, P., and ZYSS, J.: 'Cascading of 2nd order nonlinear processes in waveguides'. Proceedings ECIO'95, Delft, 1995, pp. 335–338
11 BIEBER, A.E., PRELEWITZ, D.F., BROWN, T.G., and TIBERIO, R.C.: 'Optical switching in a metal-semiconductor-metal waveguide structure', *Appl. Phys. Lett.,* 1995, **66**, pp. 3401–3403
12 LIU, M.Y., XIAO, X., PRUCNAL, P.R., and STURM, J.C.: 'All-optical switching in an asymmetric silicon Fabry-Perot Étalon based on the free-carrier plasma effect', *Appl. Opt.,* 1994, **33**, pp. 3871–3874
13 HENARI, F.Z., MORGENSTERN, K., BLAU, W., KARAVANSKII, V.A., and DNEPROVSKII, V.S.: 'Third-order optical nonlinearity and all-optical switching in porous silicon', *Appl. Phys. Lett.,* 1995, **67**, pp. 323–325
14 SHIMADA, S., NAKAGAWA, K., SARUWATARI, M., and MATSUMOTO, T.: 'Very-high-speed optical signal processing', *Proc. IEEE,* 1993, **81**, pp. 1633–1646
15 RATOVELOMANANA, F., VODJDANI, N., ENARD, A., GLASTRE, G., RONDI, D., BLONDEAU, R., JOERGENSON, C., DURHUUS, T., and MIKKELSEN, B.: 'An all-optical wavelength-converter with semiconductor optical amplifiers monolithically integrated in an asymmetric passive Mach-Zehnder interferometer', *IEEE Photonics Technol. Lett.,* 1995, **7**, pp. 992–994
16 KROL, D.M., and THAKUR, M.: 'Measurement of the nonlinear refractive index of single-crystal polydiacetylene channel waveguides', *Appl. Phys. Lett.,* 1990, **56**, pp. 1406–1408
17 MOLYNEUX, S., KAR, A.K., WHERRET, B.S., AXON, T.L., and BLOOR, D.: 'Near-resonant refractive nonlinearity in polydiacetylene 9-BCMU thin films', *Opt. Lett.,* 1993, **18**, pp. 2093–2095
18 HATTORI, K., KITAGAWA, T., OGUMA, M., WADA, M., TEMMYO, J., and HORIGUCHI, M.: 'Erbium-doped silica-based planar waveguide amplifiers pumped by 0.98μm laser diodes', *Electron. Lett.,* 1993, **29**, pp. 357–359
19 VAN WEERDEN, H.J., HOEKSTRA, T.H., LAMBECK, P.V., and POPMA, TH.J.A.: 'Low-threshold amplification at 1.5μm in Er:Y_2O_3 IO-amplifiers'. Proc. ECIO'97, Stockholm, 1997, pp. 169–172
20 MYSLINSKI, P., BARNARD, C.W., and CHROSTOWSKI, J.: 'Remote all-optical nanosecond gain switching of an erbium-doped fiber amplifier', *Fiber Integr. Opt.,* 1995, **14**, pp. 83–88
21 HOEKSTRA, H.J.W.M.: 'On beam propagation methods for modeling in integrated optics', *Opt. Quantum Electron.,* 1997, **29**, pp. 157–171
22 KRIJNEN, G.J.M., HOEKSTRA, H.J.W.M., STEGEMAN, G.I., and TORUELLAS, W.: 'Cerenkov second-harmonic generation in the strong conversion limit: new effects', *Opt. Lett.,* 1996, **21**, pp. 851–853
23 KRIJNEN, G.J.M., HOEKSTRA, H.J.W.M., and LAMBECK, P.V.: 'A new method for the calculation of propagation constants and field profiles of guided modes of nonlinear channel waveguides based on the effective index method', *J. Lightwave Technol.,* 1994, **12**, pp. 1550–1559
24 HORST, F., HOEKSTRA, H.J.W.M., DRIESSEN, A., and POPMA, TH.J.A.: 'Time domain propagation method for the simulation of temporal solitons in periodic media'. Proceedings LEOS '95, San Francisco, 1995, Vol. 2, pp. 27–28
25 HORST, F., HOEKSTRA, H.J.W.M., DRIESSEN, A., and POPMA, TH.J.A.: 'Simulation of a self-switching nonlinear Bragg reflector using realistic nonlinear parameters'. Proceedings CLEO/Europe, Hamburg, 1996, Paper CTuK62
26 HORST, F.: 'Soliton switching in an integrated optical nonlinear Bragg reflector'. Ph.D Thesis, Enschede 1997
27 KRIJNEN, G.J.M.: 'All-optical Switching in Nonlinear Integrated Optic Devices'. Ph.D Thesis, Enschede 1992
28 KRIJNEN, G.J.M., VILLENEUVE, A., STEGEMAN, G., AITCHISON, S., LAMBECK, P.V., and HOEKSTRA, H.J.W.M.: 'Modeling of a versatile all-optical Mach-Zehnder switch' *in* TAMIR, T., and GRIFFEL, G. (Eds.): 'Guided-wave optoelectronics: Device characterization and design' (Plenum Press, 1995), pp. 187–196
29 OFFREIN, B.J.: 'The Fabry-Perot Resonator as an All-Optical Switching Device'. Ph.D Thesis, Enschede 1994
30 THAKUR, M., and KROL, D.M.: 'Demonstration of all-optical phase modulation in polydiacetylene waveguides', *Appl. Phys. Lett.,* 1990, **56**, pp. 1213–1215
31 BARTUCH, U., BRÄUER, A., DANNBERG, P., HÖRHOLD, H.H., and RAABE, D.: 'Measurement of high nonresonant third-order nonlinearity in MP-PPV waveguides', *Int. J. Optoelectron.,* 1992, **7**, pp. 275–279
32 VAN SCHOOT, J.B.P., HOEKSTRA, H.J.W.M., DRIESSEN, A., and POPMA, TH.J.A.: 'Design and realization of monomodal SiO_xN_y-based polymer waveguides for active functions'. Proceedings LEOS'95, San Francisco, 1995, Vol. 2, pp. 84–85
33 VAN SCHOOT, J.B.P.: 'Characterization and application of organic materials for all-optical integrated optic devices'. Ph.D Thesis, Enschede 1995
34 VAN SCHOOT, J.B.P., BLOM, F.C., HOEKSTRA, H.J.W.M., DRIESSEN, A., and POPMA, TH.J.A.: 'Realisation of an integrated all-optical non-linear Mach-Zehnder interferometer'. Proc. ECIO'95, Delft, 1995, pp. 209–212
35 MARQUES, M.B.: 'Large, nonresonant, intensity dependent refractive index of 4-dialkylamino-4′nitrodiphenyl-polyene side chain polymers in waveguides', *Appl. Phys. Lett.,* 1991, **58**, pp. 2613–2615
36 DRIESSEN, A., HORST, F., HOEKSTRA, H.J.W.M., VAN SCHOOT, J.B.P., and POPMA, Th.J.A.: 'Two photon absorption measurements in polymer waveguides on a picosecond timescale'. Proc. ECIO'97, Stockholm, 1997, pp. 428–431
37 DRIESSEN, A., HOEKSTRA, H.J.W.M., BLOM, F.C., HORST, F., KRIJNEN, G.J.M., VAN SCHOOT, J.B.P., LAMBECK, P.V., and POPMA, Th.J.A.: 'Evaluation of polymer based third-order nonlinear integrated optics devices', *Opt. Mater.,* 1998, **9**, pp. 329–333